AGU PUBLICATIONS

Geophysical Research Letters

RESEARCH LETTER
10.1002/2015GL064479

Key Points:
- Aerosols contribute to flooding by "aerosol-enhanced conditional instability"
- Reducing pollution (particularly BC) in the Sichuan Basin mitigates floods
- Coupling aerosols with meteorology may improve weather forecasts

Supporting Information:
- Texts S1 and S2, Table S1, and Figures S1–S4

Correspondence to:
J. Fan,
Jiwen.Fan@pnnl.gov

Citation:
Fan, J., D. Rosenfeld, Y. Yang, C. Zhao, L. R. Leung, and Z. Li (2015), Substantial contribution of anthropogenic air pollution to catastrophic floods in Southwest China, *Geophys. Res. Lett.*, *42*, 6066–6075, doi:10.1002/2015GL064479.

Received 6 MAY 2015
Accepted 18 JUN 2015
Accepted article online 21 JUN 2015
Published online 20 JUL 2015

Substantial contribution of anthropogenic air pollution to catastrophic floods in Southwest China

Jiwen Fan[1], Daniel Rosenfeld[2], Yan Yang[1,3], Chun Zhao[1], L. Ruby Leung[1], and Zhanqing Li[4,5]

[1]Atmospheric Sciences and Global Change Division, Pacific Northwest National Laboratory, Richland, Washington, USA, [2]Institute of Earth Sciences, Hebrew University of Jerusalem, Jerusalem, Israel, [3]Chinese Academy of Meteorological Sciences, Beijing, China, [4]Department of Atmospheric and Oceanic Science and ESSIC, University of Maryland, College Park, Maryland, USA, [5]State Key Laboratory of Earth Surface Processes and Resource Ecology and Joint Center for Global Change Studies, Beijing Normal University, Beijing, China

Abstract Extreme weather events have become more frequent and are likely linked to increases in greenhouse gases and aerosols, which alter the Earth's radiative balance and cloud processes. On 8–9 July 2013, a catastrophic flood devastated the mountainous area to the northwest of the Sichuan Basin. Atmospheric simulations at a convection-permitting scale with aerosols and chemistry included show that heavy air pollution trapped in the basin significantly enhances the rainfall intensity over the mountainous areas through "aerosol-enhanced conditional instability." That is, aerosols suppress convection by absorbing solar radiation and increasing atmospheric stability in the basin during daytime. This allows excess moist air to be transported to the mountainous areas and orographically lifted, generating strong convection and extremely heavy precipitation at night. We show that reducing pollution in the Sichuan Basin can effectively mitigate floods. It is suggested that coupling aerosol with meteorology can be crucial to improve weather forecast in polluted regions.

1. Introduction

Changes in extreme weather and climate events have been observed in many regions since the 1950s [*Intergovernmental Panel on Climate Change* (*IPCC*), 2013; *Peterson et al.*, 2013]. Global warming due to increased greenhouse gas emissions may increase the occurrence of extreme events [*Peterson et al.*, 2013]. Human activities also produce more pollution particles that influence surface and atmospheric temperatures by scattering or absorbing solar radiation [*Li*, 1998; *Bollasina et al.*, 2011; *Menon et al.*, 2002; *Ramanathan et al.*, 2005; *Lau et al.*, 2006; *Lau and Kim*, 2006; *H. Zhang et al.*, 2009; *Bollasina et al.*, 2013; *Bond et al.*, 2013]. This is referred to as the aerosol-radiation interaction (ARI) in the *IPCC* [2013] report. Aerosol particles can also act as cloud condensation nuclei (CCN) or ice nuclei (IN) [*Fan et al.*, 2010; *Tao et al.*, 2012; *Fan et al.*, 2013]. This is referred to as the aerosol-cloud interaction (ACI) in the *IPCC* [2013] report.

These aerosol effects may modify convection, atmospheric stability, and circulation, which influence weather and climate [*Lau et al.*, 2006; *Bollasina et al.*, 2011; *Fan et al.*, 2012; *Bollasina et al.*, 2013; *Bond et al.*, 2013]. In a tropical sea breeze convective event, aerosols can enhance convection at night through aerosol-cloud-land surface interactions [*Grant and van den Heever*, 2014]. The aerosol direct effect of absorbing aerosols can reduce premonsoon precipitation by reducing surface temperature which stabilizes the atmosphere [*Lee et al.*, 2014]. Earlier onsets of South and East Asian monsoons and increased rainfall over the Indian subcontinent have been linked to the absorbing aerosols over the Indo-Gangetic Plain [*Lau and Kim*, 2006]. Some studies have also suggested that aerosols can significantly impact severe weather by modifying hurricanes and tropical cyclones [*Rosenfeld et al.*, 2012; *Wang et al.*, 2014b] and enhancing the intensities of storm track and winter cyclones over the northwestern Pacific [*Zhang et al.*, 2007; *Wang et al.*, 2014a]. Recently, *Saide et al.* [2015] have found that smoke aerosols can promote tornadogenesis and increase tornado intensity and longevity by enhancing the capping inversion. However, the contribution of pollution particles to extreme weather is highly uncertain due to lack of measurements and difficulties in parameterizing the ARI and the ACI in large-scale models [*Zhang and Wang*, 2011; *Wang*, 2013; *Lim et al.*, 2014].

In regions with heavy anthropogenic pollution such as China and India, increases in the frequencies and intensities of floods and droughts have been observed over the past few decades [*Yao et al.*, 2008; *Ye et al.*, 2013; *Fu and Dan*, 2014; *Sheikh et al.*, 2014]. Over China, the "northern drought/southern flooding"

phenomenon has also been linked to black carbon (BC) in the atmosphere [*Menon et al*., 2002], although the simulated aerosol absorption was found to be much stronger than the observed aerosol absorption [*Lee et al*., 2007]. Absorbing aerosols have been linked to the suppression of heavy rainfall in central China [*Yang et al*., 2013], while an enhancement of heavy thunderstorms has been found to be associated with hygroscopic aerosols in southeast China [*Yang and Li*, 2014]. The invigoration of convection and precipitation through the ACI for hygroscopic aerosols (i.e., effective CCN) has been reported in many other studies [e.g., *Khain et al*., 2005; *Rosenfeld et al*., 2008; *Li et al*., 2011], but it is generally associated with hygroscopic aerosols having number concentrations not exceeding an optimal value [*Wang* 2005; *Fan et al*., 2007; *Li et al*., 2008]. *Fan et al*. [2008] have shown that as the aerosol absorption capability increases, the invigoration of convective intensity and precipitation through the ACI could turn into suppression through the ARI.

Pollution over the Sichuan Basin is especially severe due to the nearly closed deep basin topography and the rapid urbanization and industrialization experienced in recent decades [*Chen et al*., 2014]. This has resulted in a much larger aerosol optical depth (AOD) and negative surface direct forcing in summer compared with other regions of China [*Qian et al*., 2003; *Li et al*., 2010; *Chen et al*., 2014]. Black carbon is the major contributor to air pollution over the basin [*Qian et al*., 2003; *Chen et al*., 2014]. Floods have become more frequent in summertime over Southwest China in recent decades [*Ye et al*., 2013]. The 2013 Southwest China flood that occurred on 8–9 July 2013 was the worst in five decades. Beichuan County (BCH), which is located in the mountainous regions northwest of the Sichuan Basin, suffered the most damage. There were ~30 cm of rain within 24 h from 0800 LST 8 to 9 July at Dujiangyan. The major synoptic system associated with the flood, shown in Figure S1a in the supporting information (SI), was a cutoff upper airflow of the jet stream with a strong upper level low that formed a strong and persistent upper level disturbance. This was conducive to the transport of lower level moisture by the monsoonal flow into the south and west regions of China from the Indian Ocean and India, Bangladesh, Thailand, and Vietnam. But why was the flood so catastrophic in the mountainous regions of Sichuan? Did the heavy anthropogenic pollution over the Sichuan Basin play a role in the flooding?

To answer these questions, we carried out model simulations of the catastrophic flood event and associated sensitivity simulations in this study. Ensemble simulations with five ensemble members initialized at different times of 6 h apart (see supporting information for details) were conducted at a convection-permitting scale (3 km) using the improved chemistry version of the Weather Research and Forecasting (WRF) model (WRF-Chem) [*Skamarock et al*., 2008; *Zaveri et al*., 2008; *Zhao et al*., 2010]. The simulations covered a regional domain of 1800 km × 1650 km centered at the Sichuan Basin (red box in Figure S1b), with 40 vertical levels up to 50 hPa. Simulations with current industrial emissions [*Q. Zhang et al*., 2009] are referred to as P_ALL (Table S1 in supporting information). To explore the contribution of anthropogenic pollution to the flood, current industrial emissions were reduced to a level that is close to that of the late 1970s and early 1980s before the China economic boom began, following *Bennartz et al*. [2011]. This is referred to as C_ALL (Table S1). To isolate the contributions of the ARI and the ACI, P_NORAD and C_NORAD were conducted by excluding ARI based on P_ALL and C_ALL, respectively. More details about the model and experiments are included in Text S1 in supporting information. All results, including those from the sensitivity tests, are based on the ensemble means. Time shown in this paper is the local standard time (LST, UTC + 8).

2. Results

Using current industrial emissions (P_ALL), model simulations, with both ARI and ACI effects included, capture the location and intensity of the heavy rain that was measured by rain gauges from 08:00 LST on 8 July to 07:00 LST on 9 July 2013 (Figures 1a and 1b). The observed strong storm at BCH begins at 21:00 LST on 8 July and ends at ~05:00 LST on 9 July. Only P_ALL captures the intense precipitation rates well (red line in Figure 1f). The observed heavy precipitation over the mountainous regions of Sichuan is captured by the simulation (Figures 1a versus 1b), showing extremely heavy rain over BCH. Simulated AOD generally agrees with satellite retrievals over the Sichuan Basin (Figures S2a versus S2b). Although P_ALL overestimates AOD in the northeastern region of the domain, this should not impact our results since that region is not in the circulation system we examined. The large AOD (up to 0.9) and high aerosol number mixing ratio ($> 10^{11}\,kg^{-1}$) in the Sichuan Basin suggest a very strongly absorbing polluted environment in P_ALL. This falls in the extreme ARI-dominant regime under which convection should be severely

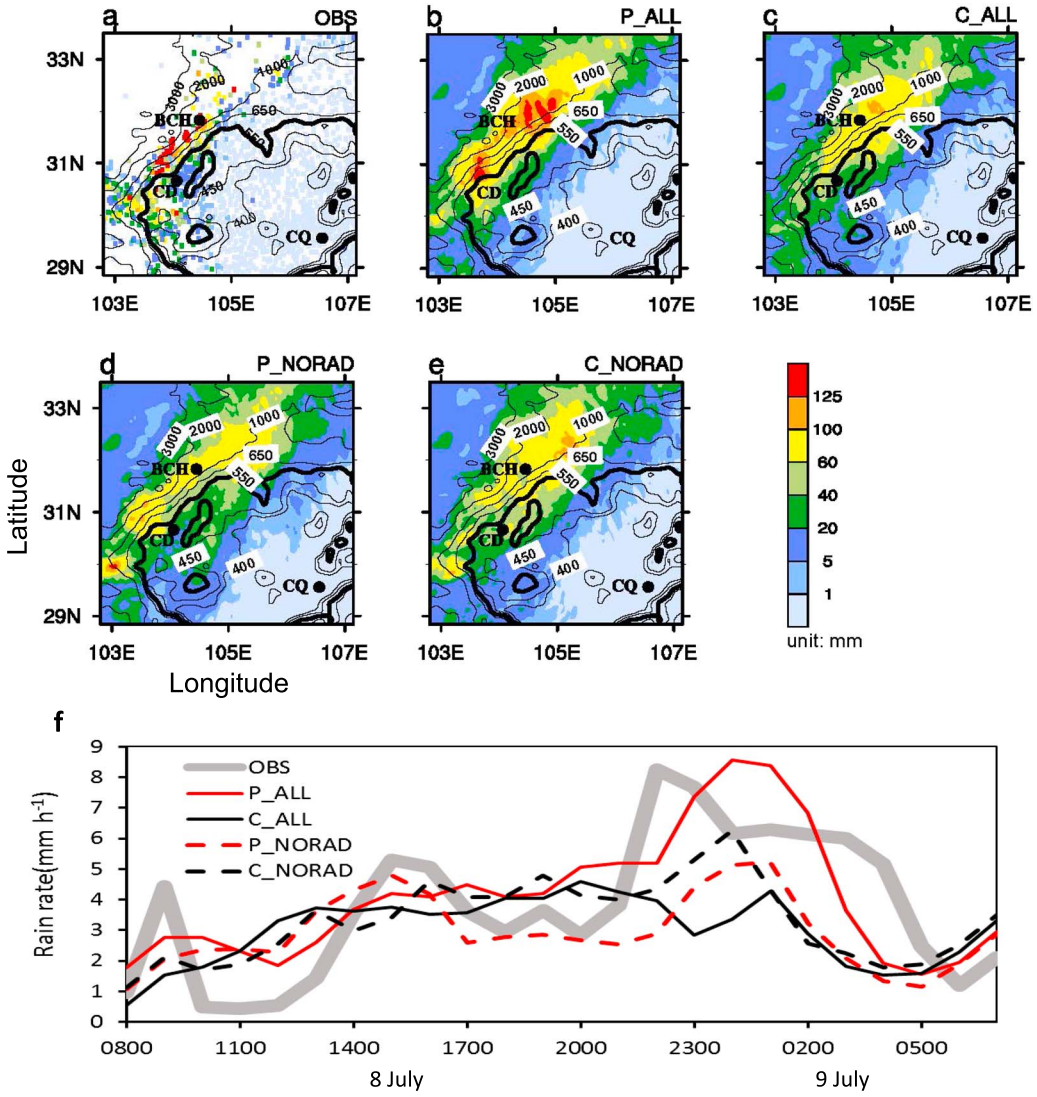

Figure 1. Accumulated precipitation during the period 20:00 LST on 8 July to 07:00 LST 9 July (the main storm period) from (a) rain gauge observations, (b) P_ALL, (c) C_ALL, (d) P_NORAD, and (e) C_NORAD. (f) The time series of rain rate for P_ALL (the red line), C_ALL (the black line), P_NORAD (the red dashed line), and rain gauge observation (the green line) averaged over Beichuan County (BCH, 103.8°E to 104.8°E, 31.5°N to 32°N) where the heaviest rain was observed. Note that the observations in Figure 1f (the gray line) are the mean values of measurements made at 19 stations in BCH, which may not well represent the domain mean. The black contours in Figures 1a–1d are the terrain heights of 400, 450, 550 (bold), 650, 1000, 2000, and 3000 m. Acronyms: CD (Chengdu) and CQ (Chongqing).

suppressed, according to *Rosenfeld et al.* [2008]. The airflow of the lower atmosphere is mainly southerly and southwesterly, and the simulation captures the circulation patterns and generally simulates the wind direction and magnitude, as well as the time evolution of the wind fields (Figures S2d and S2e).

When the current industrial emissions are reduced to the level before the China economic boom began (C_ALL), the air becomes much cleaner with AOD in the Sichuan Basin generally less than 0.3 (Figure S2c). The precipitation over the mountainous regions is reduced by 15–45% compared to P_ALL (Figures 1c versus 1b). Averaged over the entire county of BCH, the rain rate is reduced by about 20–60% during the main storm period (i.e., 20:00 LST on 8 July to 07:00 LST on 9 July) (Figure 1f). The region with the heaviest precipitation (>100 mm) during that period almost totally disappears in C_ALL (Figure 1c). This shows the remarkable contribution of anthropogenic emissions to the extreme precipitation. The catastrophic floods might not have occurred had the air pollution level been lower, even though widespread precipitation would have still occurred over the mountains due to the meteorological conditions present at the time.

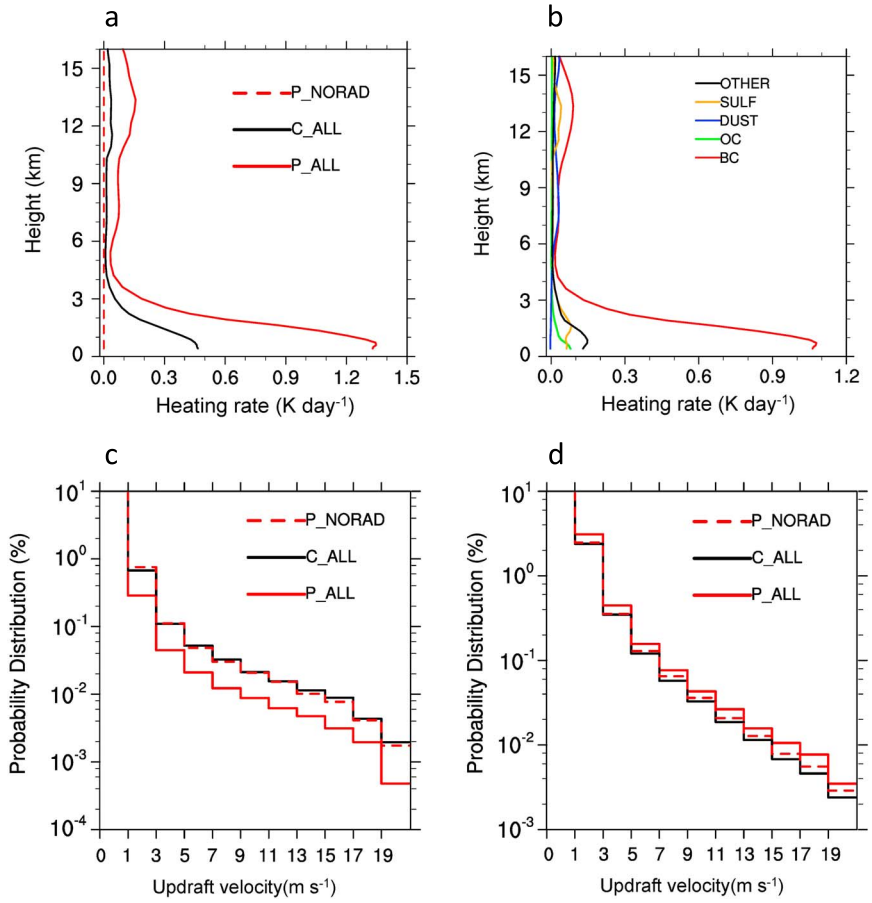

Figure 2. Vertical profiles of (a) total aerosol heating rate from P_ALL (the red line), C_ALL (the black line), and P_NORAD (the red dashed line) and (b) heating rates from dust, organic carbon, and black carbon (BC) in P_ALL. (c and d) The probability distribution frequency (PDF, %) of the updraft velocity over the basin from 14:00 to 20:00 LST on 8 July, and over the mountains from 20:00 LST on 8 July to 07:00 LST on 9 July, respectively, from C_ALL (the black line), P_ALL (the red line), and P_NORAD (the red dashed line). The heating rates in Figures 2a and 2b are calculated for clear-sky columns (each grid within the column has a total condensate mass ratio of less than 10^{-6} kg kg^{-1}) and averaged over the domain of the red box marked in Figure S1c and over the daytime of 8 July (i.e., 08:00–20:00 LST).

To isolate the ARI from the ACI related to the effect of CCN in this study (the IN effect is not considered), the P_ALL simulations are repeated with the ARI turned off (P_NORAD; Table S1). The precipitation amount and spatial pattern resemble those under the clean environment (Figures 1d versus 1c). This suggests that the ARI is mainly responsible for the greatly enhanced precipitation over the mountain region in the polluted environment. To further validate the small contribution of the ACI, the C_ALL simulations are also repeated with the ARI turned off (C_NORAD; Table S1). The precipitation of C_NORAD is very similar to C_ALL since ARI is small under the clean environment (Figures 1e versus 1c), so only C_ALL is included for later discussion. A comparison between P_NORAD and C_NORAD suggests that the ACI here slightly decreases the precipitation amount and delays the peak precipitation by about 1 h (Figure 1f). Note that the ACI effect from C_ALL to P_ALL might not be the same. The contribution of the ARI to the enhanced precipitation is dominant due to the strong absorption of aerosols as shown in Figure 2a. This is consistent with previous studies that have shown that the ARI dominates over the ACI under high AOD conditions [*Rosenfeld et al.*, 2008] and strongly absorbing aerosol environments [*Fan et al.*, 2008].

To explore the mechanism behind how the ARI enhances precipitation over the mountainous area of Sichuan, we first examine the aerosol distribution and air mass origins. Under a clear sky or a sky with thin clouds, BC is the dominant absorber of solar radiation in the lower atmosphere over the region (Figure 2b). BC emissions are mainly located in the Sichuan Basin and at Guiyan, which is southeast of Sichuan ("GY" in Figure S1c). Back trajectories show that air originating from the GY region takes more than 24 h to reach

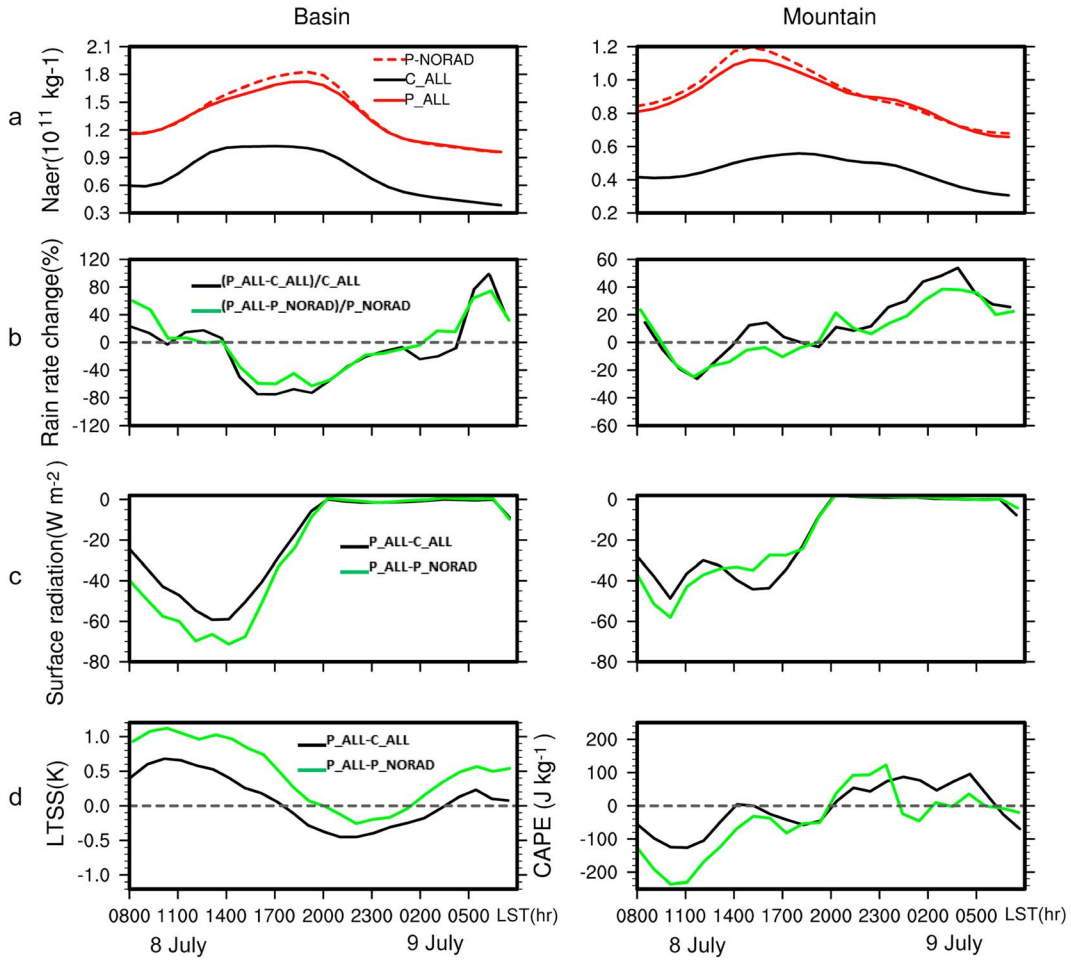

Figure 3. Time series of (a) column-integrated aerosol number mixing ratio (N_{aer}) from P_ALL (the red line), C_ALL (the black line), and P_NORAD (the red dashed line), (b) rain rate change between P_ALL/C_ALL (the black line) and P_ALL/P_NORAD (the green line; e.g., (P_ALL -C_ALL)/C_ALL*100%), (c) differences in net surface radiation between P_ALL/C_ALL (the black line) and P_ALL/P_NORAD (the green line), and (d) differences in lower tropospheric static stability (LTSS) between P_ALL/C_ALL (the black line) and P_ALL/P_NORAD (the green line) over the (left) basin and convective available potential energy over the (right) mountains. LTSS is calculated using the potential temperature differences between the maximum aerosol heating level (~1.7 km) and the lowest model level (~30 m). Due to the complex topography and high terrain height over the mountains, CAPE is calculated instead of LTSS. Rain rates are averages over grid points with rain rates larger than 0.25 mm h^{-1}. Other quantities are averaged over clear-sky grid points, which are defined as those grid points with total condensate mass ratios of less than 10^{-6} kg kg^{-1}.

mountainous areas of Sichuan such as BCH (Figure 4a). However, at around 08:00 LST on 8 July, which is 12 h before the main storm period, the precipitation, moist static energy (MSE), water vapor, and temperature conditions in the polluted environment (P_ALL) are very similar to those in C_ALL and P_NORAD. By further examining those quantities from the previous day (7 July), we see significant differences between P_ALL and C_ALL (P_NORAD) in the daytime but smaller differences at night. This suggests that the daytime ARI effect due to the absorption of sunlight in P_ALL diminishes at night due to precipitation processes, so little difference is carried over to the next day. Hence, within the 12 h before the main storm period, air that reaches the mountains originates from the Sichuan Basin.

We therefore focus our analysis on the airflow from the basin to the mountains on 8 July. The basin and mountain areas are separated by a terrain height of 550 m for further analysis (bold black curve in Figure S3 and other figures with topography). During the 12 h before sunset, i.e., 20:00 LST on 8 July, air reaching the mountains travels over the basin. During the main storm period, the enhanced precipitation in P_ALL compared to C_ALL and P_NORAD occurs over the mountains (Figures 1 and S3a), with small differences in the basin of about −4% relative to C_ALL and ~7% relative to P_NORAD (Figures 1b versus 1c). However, in

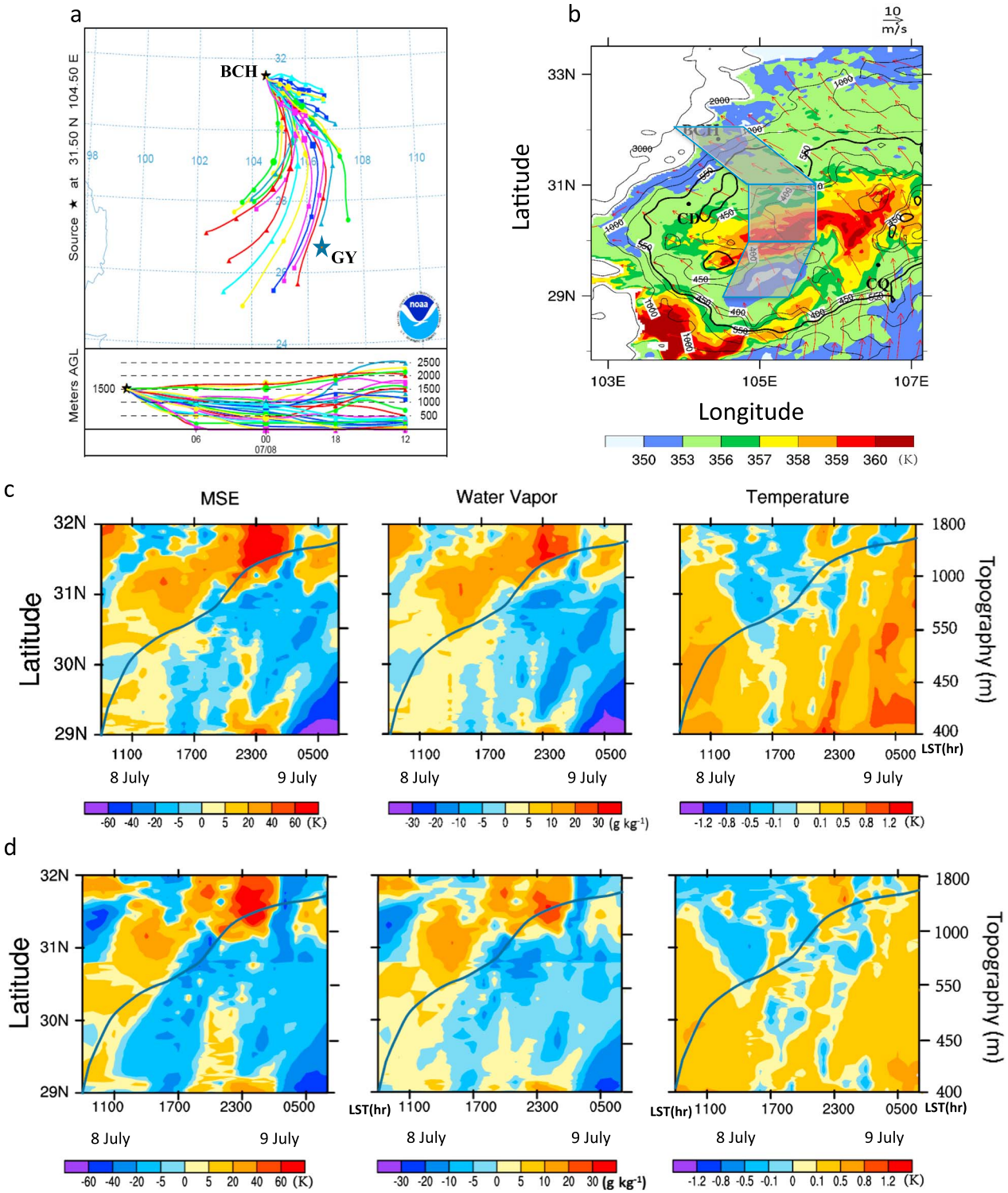

Figure 4. (a) The 24 h backward trajectories of the wind fields ending at Beichuan (BCH) at 20:00 LST on 8 July and (b) moist static energy (MSE) at 17:00 LST on 8 July with the wind field at 800 hPa from P_ALL. The gray shaded area (20 grid points or 60 km wide) in Figure 4b represents the airflow path that is used for plotting Figures 4c and 4d. The trajectories were calculated using HYSPLIT based on the Global Data Assimilation System with 1° resolution, which is from NCEP 1° data. We compared the NCEP and P_ALL wind fields, and they are consistent in terms of wind direction and intensity. (c) Differences in MSE (left), water vapor (middle), and temperature (right) between P_ALL and C_ALL along the airflow trajectories marked in Figure 4b as a function of time and latitude. (d) The same as Figure 4c except for differences between P_ALL and P_NORAD. MSE and water vapor are integrated between the surface and 8 km and averaged over the shaded area in Figure 4b. The temperature plot shows temperatures at 1.5 km, which is close to the height at which the maximum in aerosol heating occurs. It is also averaged over the shaded area in Figure 4b. The gray line denotes the topography (the secondary *y* axis on the right) as a function of time along the airflow path (averaged over the shaded area).

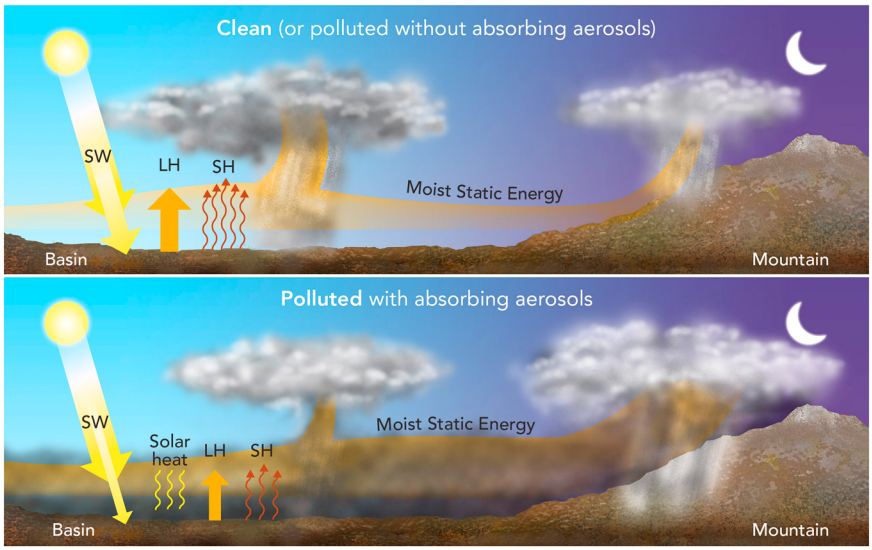

Figure 5. Illustration of the mechanism called aerosol-enhanced conditional instability. In the polluted case with strong absorbing aerosols (P_ALL), greater amounts of MSE build up over the Sichuan Basin during daytime because convection is largely suppressed by the ARI compared to the clean case (C_ALL) or the polluted case without the ARI (P_NORAD). For the latter two cases, (top) the much smaller ARI allows the stronger convection to consume much more MSE over the basin. (bottom) The excess MSE in the polluted case is transported to the mountainous area by the prevailing winds and orographically lifted, generating much stronger convection and precipitation over the mountain at night. Acronyms: MSE (moist static energy), SW (shortwave radiation), SH (surface sensible heat flux), and LH (surface latent heat flux).

the afternoon before the main storm period (14:00–20:00 LST; Figure S3b), precipitation in the basin is suppressed in P_ALL (by −60% compared with C_ALL and −45% compared with P_NORAD), while the differences over the mountains are small (not shown). The precipitation suppression in the basin is associated with much weaker convection (Figure 2c) caused by the greater atmospheric stability induced by ARI during the daytime (Figure 3d, left). The clear-sky aerosol concentration in the basin is ~2–3 times higher in P_ALL compared with C_ALL (Figure 3a), and aerosol heating is ~4 times stronger at the ~1 km altitude (Figure 2a). The ARI greatly stabilizes the atmosphere over the basin by (1) reducing surface radiation (Figure 3c), which cools the surface and leads to reduced sensible and latent heat fluxes (Figure S4), weakening convection [e.g., *Lee et al.*, 2014] and (2) heating the lower atmosphere at 1–2 km and reducing the corresponding relative humidity, as well as the temperature contrast to the surface, which is seen in this analysis and has been noted in previous studies [e.g., *Feingold et al.*, 2005; *Fan et al.*, 2008]. Therefore, compared with C_ALL (or P_NORAD), less MSE is consumed in P_ALL during daytime in the basin due to much weaker convection. The MSE accumulates over time due to (1) the warming by aerosol absorption of solar radiation and (2) the lesser removal by precipitation during the daytime. The excess MSE is transported toward the mountains by the prevailing winds. Figures 4c and 4d show the transport and accumulation of MSE toward the mountains with time. It also shows that over the basin, the excess MSE is primarily from excess water vapor, the result of a more stable atmosphere. Compared with C_ALL and P_NORAD, P_ALL has higher temperatures over the basin but slightly colder temperatures over the mountains during all times at an altitude of ~1.5 km. This is likely due to weaker (stronger) convection and precipitation in the basin (mountains). As the air that carries the larger MSE reaches the mountains at night, the orographic uplift of the air with a larger convective available potential energy (CAPE) (Figure 3d, right) generates significantly stronger storms (Figure 2d) with a mean maximum vertical velocity of 21.1 m s^{-1} averaged over the main storm period (versus 17.5/18.9 m s^{-1} in C_ALL/P_NORAD). This leads to more extreme precipitation. This "aerosol-enhanced conditional instability" induced by absorbing aerosols is summarized schematically in Figure 5.

3. Discussion

We propose a mechanism called "aerosol-enhanced conditional instability," by which strongly absorbing aerosols increase convection and precipitation downwind of a heavily polluted area. This effect could

escalate convective events to severe weather events, particularly in downwind mountainous areas that provide an additional lifting or convective triggering. We have shown that reducing pollution, particularly absorbing aerosols, in polluted areas would effectively mitigate the extreme precipitation in downwind areas. For the Sichuan flooding event, the main absorbing aerosol species present in the atmosphere was BC, which is generated from human activities. BC not only brings about health and environmental problems but also has major climate implications, as revealed by *Menon et al*. [2002]. It is now linked to extreme weather events.

Although some parts of the mechanism have been extensively studied in previous work such as the enhanced boundary layer stability by absorbing aerosols [e.g., *Ramanathan et al*., 2005; *Feingold et al*., 2005; *Fan et al*., 2008; *Cherian et al*., 2013], and a few past studies have also shown that aerosols can impact severe weather features such as tropical cyclones and tornadoes [*Wang et al*., 2014b; *Saide et al*., 2015], this study shows a mechanism that can have a remote effect on precipitation in a relatively pristine area downwind of a polluted environment and how it can foster an extreme weather event when a triggering mechanism such as orographic lifting exists. While this finding was discovered in Southwest China, the mechanism proposed might apply to many other regions in the world with similar topographies and pollution levels (e.g., the Ganges Plain in India and Los Angeles in the United States). However, the proposed mechanism is associated with atmospheric circulation on a synoptic scale and extreme precipitation events, so it may not be generalized to precipitation influenced by local-scale mountain-valley circulations. This study suggests that the coupling of aerosols with meteorology could be crucial for improving weather forecasts in polluted regions. A recent study by *Saide et al*. [2015] in which biomass burning smoke was found to increase the severity of tornadoes by enhancing the capping inversion through radiation absorption also highlighted the need to consider the feedback of aerosols in numerical severe weather forecasting.

Increased precipitation was previously found in urban downwind regions through aerosol indirect effects related to CCN [*Van den Heever and Cotton*, 2007; *Carrió et al*., 2010; *Han et al*., 2012]. In this study, however, it is produced by ARI due to the strong absorbing nature of aerosols in the Sichuan Basin through the mechanism of aerosol-enhanced conditional instability. The ACI, i.e., the so-called aerosol indirect effect, is shown to be small in this study because of the large amount of BC and very high aerosol number concentrations over the Sichuan Basin. Although hygroscopic aerosols such as sulfate could have strong indirect effects by serving as CCN, thereby significantly invigorating clouds and precipitation [e.g., *Khain et al*., 2005; *Rosenfeld et al*., 2008; *Li et al*., 2011; *Fan et al*., 2013], with a high AOD of ~0.9 over the Sichuan Basin, the ARI should be dominant over the ACI there, based on theoretical calculations done by *Rosenfeld et al*. [2008]. The two-moment bulk scheme used in this study might add some uncertainty to the ACI results because of parameterization limitations in the bulk scheme (e.g., the saturation adjustment approach for condensation, size sorting problems, etc.), the main point of this study would not be affected, as *Fan et al*. [2008], in which a bin cloud microphysical scheme instead of a bulk cloud microphysical scheme was used, have demonstrated the dominant effects of the ARI on convection and precipitation under strong aerosol absorption conditions.

Acknowledgments

This study was supported by the U.S. Department of Energy (DOE) Office of Science Biological and Environmental Research as part of the Regional and Global Climate Modeling program (RGCM), and the Ministry of Science and Technology (2013CB955804). The Pacific Northwest National Laboratory (PNNL) is operated for the DOE by Battelle Memorial Institute under contract DE-AC06-76RLO1830. The model simulations were performed using PNNL Institutional Computing. The model and observational data can be obtained by contacting Jiwen.Fan@pnnl.gov.

The Editor thanks two anonymous reviewers for their assistance in evaluating this paper.

References

Bennartz, R., J. Fan, J. Rausch, L. R. Leung, and A. K. Heidinger (2011), Pollution from China increases cloud droplet number, suppresses rain over the East China Sea, *Geophys. Res. Lett.*, *38*, L09704, doi:10.1029/2011GL047235.

Bollasina, M. A., Y. Ming, and V. Ramaswamy (2011), Anthropogenic aerosols and the weakening of the south Asian summer monsoon, *Science*, *334*, 502–505, doi:10.1126/science.1204994.

Bollasina, M. A., Y. Ming, and V. Ramaswamy (2013), Earlier onset of the Indian monsoon in the late twentieth century: The role of anthropogenic aerosols, *Geophys. Res. Lett.*, *40*, 3715–3720, doi:10.1002/grl.50719.

Bond, T. C., et al. (2013), Bounding the role of black carbon in the climate system: A scientific assessment, *J. Geophys. Res. Atmos.*, *118*, 5380–5552, doi:10.1002/jgrd.50171.

Carrió, G. G., W. R. Cotton, and W. Y. Y. Cheng (2010), Urban growth and aerosol effects on convection over Houston: Part 1. The August 2000 case, *Atmos. Res.*, *96*, 560–574, doi:10.1016/j.atmosres.2010.01.005.

Chen, Y., S. Xie, B. Luo, and C. Zhai (2014), Characteristics and origins of carbonaceous aerosol in the Sichuan Basin, China, *Atmos. Environ.*, *94*, 215–223, doi:10.1016/j.atmosenv.2014.05.037.

Cherian, R., C. Venkataraman, J. Quaas, and S. Ramachandran (2013), GCM simulations of anthropogenic aerosol-induced changes in aerosol extinction, atmospheric heating and precipitation over India, *J. Geophys. Res. Atmos.*, *118*, 2938–2955, doi:10.1002/jgrd.50298.

Fan, J., R. Zhang, G. Li, and W.-K. Tao (2007), Effects of aerosols and relative humidity on cumulus clouds, *J. Geophys. Res.*, *112*, D14204, doi:10.1029/2006JD008136.

Fan, J., R. Zhang, W.-K. Tao, and K. I. Mohr (2008), Effects of aerosol optical properties on deep convective clouds and radiative forcing, *J. Geophys. Res.*, *113*, D08209, doi:10.1029/2007JD009257.
Fan, J., J. M. Comstock, and M. Ovchinnikov (2010), The cloud condensation nuclei and ice nuclei effects on tropical anvil characteristics and water vapor of the tropical tropopause layer, *Environ. Res. Lett.*, *5*, 044005, doi:10.1088/1748-9326/5/4/044005.
Fan, J., D. Rosenfeld, Y. Ding, L. R. Leung, and Z. Li (2012), Potential aerosol indirect effects on atmospheric circulation and radiative forcing through deep convection, *Geophys. Res. Lett.*, *39*, L09806, doi:10.1029/2012GL051851.
Fan, J., L. R. Leung, D. Rosendeld, Q. Chen, Z. Li, H. Yu, and J. Zhang (2013), Microphysical effects determine macrophysical response for aerosol impacts on deep convective clouds, *Proc. Natl. Acad. Sci. U.S.A.*, *110*, E4581–E4590, doi:10.1073/pnas.1316830110.
Feingold, G., H. Jiang, and J. Y. Harrington (2005), On smoke suppression of clouds in Amazonia, *Geophys. Res. Lett.*, *32*, L02804, doi:10.1029/2004GL021369.
Fu, C. B., and L. Dan (2014), Trends in the different grades of precipitation over south China during 1960–2010 and the possible link with anthropogenic aerosols, *Adv. Atmos. Sci.*, *31*(2), 480–491, doi:10.1007/s00376-013-2102-7.
Grant, L. D., and S. C. van den Heever (2014), Aerosol-cloud-land surface interactions within tropical sea breeze convection, *J. Geophys. Res. Atmos.*, *119*, 8340–8361, doi:10.1063/1.4803376.
Han, J.-Y., J.-J. Baik, and A. P. Khain (2012), A numerical study of urban aerosol impacts on clouds and precipitation, *J. Atmos. Sci.*, *69*, 504–520, doi:10.1175/JAS-D-11-071.1.
Intergovernmental Panel on Climate Change (IPCC) (2013), *Climate Change 2013: The Physical Science Basis. Contribution of Working Group I to the Fifth Assessment Report of the Intergovernmental Panel on Climate Change*, edited by T. F. Stocker et al., pp. 1535, Cambridge Univ. Press, Cambridge, U. K., and New York.
Khain, A., D. Rosenfeld, and A. Pokrovsky (2005), Aerosol impact on the dynamics and microphysics of deep convective clouds, *Q. J. R. Meteorol. Soc.*, *131*, 2639–2663, doi:10.1256/qj.04.62.
Lau, K.-M., and K.-M. Kim (2006), Observational relationships between aerosol and Asian monsoon rainfall, and circulation, *Geophys. Res. Lett.*, *33*, L21810, doi:10.1029/2006GL027546.
Lau, K.-M., M.-K. Kim, and K.-M. Kim (2006), Asian summer monsoon anomalies induced by aerosol direct forcing: The role of the Tibetan Plateau, *Clim. Dyn.*, *26*, 855–864, doi:10.1007/s00382-006-0114-z.
Lee, D., Y. C. Sud, L. Oreopoulos, K.-M. Kim, W. K. Lau, and I.-S. Kang (2014), Modeling the influences of aerosols on pre-monsoon circulation and rainfall over Southeast Asia, *Atmos. Chem. Phys.*, *14*, 6853–6866, doi:10.5194/acp-14-6853-2014.
Lee, K.-H., Z. Li, M.-S. Wong, J. Xin, W.-M. Hao, and F. Zhao (2007), Aerosol single scattering albedo estimated across China from a combination of ground and satellite measurements, *J. Geophys. Res.*, *112*, D22S15, doi:10.1029/2007JD009077.
Li, G., Y. Wang, and R. Zhang (2008), Implementation of a two-moment bulk microphysics scheme to the WRF model to investigate aerosol-cloud-interaction, *J. Geophys. Res.*, *113*, D15211, doi:10.1029/2007JD009361.
Li, Z. (1998), Influence of absorbing aerosols on the inference of solar surface radiation budget and cloud absorption, *J. Clim.*, *11*, 5–17.
Li, Z., K.-H. Lee, Y. Wang, J. Xin, and W.-M. Hao (2010), First observation-based estimates of cloud-free aerosol radiative forcing across China, *J. Geophys. Res.*, *115*, D00K18, doi:10.1029/2009JD013306.
Li, Z., F. Niu, J. Fan, Y. Liu, D. Rosenfeld, and Y. Ding (2011), Long-term impacts of aerosols on the vertical development of clouds and precipitation, *Nat. Geosci.*, *4*(12), 888–894, doi:10.1038/ngeo1313.
Lim, K.-S. J.-W., L. R. Fan, P.-L. Leung, B. Ma, C. Singh, Y. Zhao, G. Z. Zhang, and X.-L. Song (2014), Investigation of aerosol indirect effects using a cumulus microphysics parameterization with in a regional climate model, *J. Geophys. Res. Atmos.*, *119*, 906–926, doi:10.1002/2013JD020958.
Menon, S., J. Hansen, L. Nazarenko, and Y. Luo (2002), Climate effects of black carbon aerosols in China and India, *Science*, *297*, 2250–2253, doi:10.1126/science.1075159.
Peterson, T. C., et al. (2013), Monitoring and understanding changes in heat waves, cold waves, floods, and droughts in the United States: State of knowledge, *Bull. Am. Meteorol. Soc.*, *94*, 821–834, doi:10.1175/BAMS-D-12-00066.1.
Qian, Y., L. Ruby Leung, S. J. Ghan, and F. Giorgi (2003), Regional climate effects of aerosols over China: Modeling and observation, *Tellus B*, *55*, 914–934, doi:10.1046/j.1435-6935.2003.00070.x.
Ramanathan, V., V. C. Chung, D. Kim, T. W. Bettge, L. Buja, J. T. Kiehl, W. M. Washington, Q. Fu, D. R. Sikka, and M. Wild (2005), Atmospheric brown clouds: Impacts on south Asian climate and hydrological cycle, *Proc. Natl. Acad. Sci. U.S.A.*, *102*(15), 5326–5333, doi:10.1073/pnas.0500656102.
Rosenfeld, D., U. Lohmann, G. B. Raga, C. D. O'Dowd, M. Kulmala, S. Fuzzi, A. Reissell, and M. O. Andreae (2008), Flood or drought: How do aerosols affect precipitation?, *Science*, *321*, 1309, doi:10.1126/science.1160606.
Rosenfeld, D., W. L. Woodley, A. Khain, W. R. Cotton, G. Carrió, I. Ginis, and J. H. Golden (2012), Aerosol effects on microstructure and intensity of tropical cyclones, *Bull. Am. Meteorol. Soc.*, *93*, 987–1001.
Saide, P. E., S. N. Spak, R. B. Pierce, J. A. Otkin, T. K. Schaack, A. K. Heidinger, A. M. da Silva, M. Kacenelenbogen, J. Redemann, and G. R. Carmichael (2015), Central American biomass burning smoke can increase tornado severity in the U.S, *Geophys. Res. Lett.*, *42*, 956–965, doi:10.1002/2014GL062826.
Sheikh, M. M., et al. (2014), Trends in extreme daily rainfall and temperature indices over South Asia, *Int. J. Climatol.*, doi:10.1002/joc.4081.
Skamarock, W. C., W. C. Skamarock, J. B. Klemp, J. Dudhia, D. O. Gill, D. M. Barker, M. G. Duda, X.-Y. Huang, W. Wang, and J. G. Powers (2008), A description of the advanced research WRF version 3 NCAR Tech. Note NCAR/TN-4751STR.
Tao, W.-K., J.-P. Chen, Z. Li, C. Wang, and C. Zhang (2012), Impact of aerosols on convective clouds and precipitation, *Rev. Geophys.*, *50*, RG2001, doi:10.1029/2011RG000369.
van den Heever, S. C., and W. R. Cotton (2007), Urban aerosol impacts on downwind convective storms, *J. Appl. Meteorol. Climatol.*, *46*, 828–850, doi:10.1175/JAM2492.1.
Wang, C. (2005), A modeling study of the response of tropical deep convection to the increase of cloud condensation nuclei concentration: 1. Dynamics and microphysics, *J. Geophys. Res.*, *110*, D21211, doi:10.1029/2004JD005720.
Wang, C. (2013), Impact of anthropogenic absorbing aerosols on clouds and precipitation: A review of recent progresses, *Atmos. Res.*, *122*, 237–249, doi:10.1016/j.atmosres.2012.11.005.
Wang, Y., R. Zhang, and R. Saravanan (2014a), Asian pollution climatically modulates mid-latitude cyclones following hierarchical modelling and observational analysis, *Nat. Commun.*, *5*, 3098, doi:10.1038/ncomms4098.
Wang, Y., K.-H. Lee, Y. Lin, M. Levy, and R. Zhang (2014b), Distinct effects of anthropogenic aerosols on tropical cyclones, *Nat. Clim. Change*, *4*, 368–373.
Yang, X., and Z. Li (2014), Increases in thunderstorm Activity and relationships with air pollution in southeast China, *J. Geophys. Res. Atmos.*, *119*, 1835–1844, doi:10.1002/2013JD021224.

Yang, X., M. Ferrat, and Z. Li (2013), New evidence of orographic precipitation suppression by aerosols in central China, *Meteorol. Atmos. Phys.*, *119*, 17–29, doi:10.1007/s00703-012-0221-9).

Yao, C., S. Yang, W. Qian, Z. Lin, and M. Wen (2008), Regional summer precipitation events in Asia and their changes in the past decades, *J. Geophys. Res.*, *113*, D17107, doi:10.1029/2007JD009603.

Ye, M., Z. Qian, and Y. Wu (2013), Spatiotemporal evolution of the droughts and floods over China, *Acta Phys. Sin*, *62*(13), 139203, doi:10.7498/aps.62.139203.

Zaveri, R. A., R. C. Easter, J. D. Fast, and L. K. Peters (2008), Model for simulating aerosol interactions and chemistry (MOSAIC), *J. Geophys. Res.*, *113*, D13204, doi:10.1029/2007JD008782.

Zhang, H., and Z. Wang (2011), Advances in the study of black carbon effects on climate, *Adv. Clim. Change Res.*, *2*, 23–30, doi:10.3724/SP.J.1248.2011.00023.

Zhang, H., Z. L. Wang, P. W. Guo, and Z. Z. Wang (2009), A modeling study of the effects of direct radiative forcing due to carbonaceous aerosol on the climate in East Asia, *Adv. Atmos. Sci.*, *26*, 57–66, doi:10.1007/s00376-009-0057-5.

Zhang, Q., et al. (2009), Asian emissions in 2006 for the NASA INTEX-B mission, *Atmos. Chem. Phys.*, *9*, 5131–5153, doi:10.5194/acp-9-5131-2009.

Zhang, R., et al. (2007), Intensification of Pacific storm track linked to Asian pollution, *Proc. Natl. Acad. Sci. U.S.A.*, *104*(13), 5295–5299, doi:10.1073/pnas.0700618104.

Zhao, C., X. Liu, L. R. Leung, B. Johnson, S. A. McFarlane, W. I. Gustafson Jr., J. D. Fast, and R. Easter (2010), The spatial distribution of mineral dust and its shortwave radiative forcing over North Africa: Modeling sensitivities to dust emissions and aerosol size treatments, *Atmos. Chem. Phys.*, *10*, 8821–8838, doi:10.5194/acp-10-8821-2010.